

PAPER

A polarization-consistent R-matrix model: application to the photoionization of molecules

To cite this article: T Meltzer and Z Mašín 2022 *J. Phys. B: At. Mol. Opt. Phys.* **55** 035201

View the [article online](#) for updates and enhancements.

You may also like

- [Thermodynamics for higher dimensional rotating black holes with variable Newton constant](#)
Liu Zhao
- [BenchML: an extensible pipelining framework for benchmarking representations of materials and molecules at scale](#)
Carl Poelking, Felix Faber and Bingqing Cheng
- [Can oxygen vacancies in ceria surfaces be measured by O1s photoemission spectroscopy?](#)
Noemi Bosio, Andreas Schaefer and Henrik Groenbeck



IOP | ebooks™

Bringing together innovative digital publishing with leading authors from the global scientific community.

Start exploring the collection—download the first chapter of every title for free.

A polarization-consistent R-matrix model: application to the photoionization of molecules

T Meltzer¹ and Z Mašín*¹

Institute of Theoretical Physics, Faculty of Mathematics and Physics, Charles University, V Holešovičkách 2, 180 00 Prague 8, Czech Republic

E-mail: zdenek.masin@utf.mff.cuni.cz

Received 19 November 2021, revised 14 January 2022

Accepted for publication 20 January 2022

Published 23 February 2022



Abstract

We introduce a new variational R-matrix model called polarization-consistent coupled Hartree–Fock (PC-CHF). The PC-CHF model describes polarization and multi-channel effects in polyatomic molecules, whilst using a simple Hartree–Fock-like description of the ionic states. Furthermore, the model is constructed in a self-consistent manner meaning that all of the target states implied by the polarization configurations are included. The PC-CHF model is applied to three molecular targets ranging from small to intermediate i.e., H₂O, N₂O and formic acid (HCOOH) and the results are compared against other established R-matrix models as well as data from the literature.

Keywords: photoionization, molecular R-matrix, multi-channel, cross-sections, asymmetry parameters

 Supplementary material for this article is available [online](#)

(Some figures may appear in colour only in the online journal)

1. Introduction

From synchrotron experiments in the early 70's (Schmidt 1992) to recent ultrafast, strong-field experiments with attosecond temporal resolution and sub-ångström spatial resolution (Nisoli *et al* 2017), photoionization of atoms and molecules by single photons remains an active area of research as a detailed probe of multi-electron atomic and molecular dynamics.

Single photon data are required to model both non-perturbative (Bruner *et al* 2016, Uzan *et al* 2020) and perturbative (Huppert *et al* 2016, Dahlström *et al* 2013) ultrafast molecular dynamics. Despite recent progress in the development of new theoretical approaches for molecular perturbative stationary photoionization (Mašín *et al* 2020, Ruberti 2019,

Marante *et al* 2017, Toffoli and Decleva 2016, Toffoli and Decleva 2012) construction of accurate and readily available *ab initio* models of photoionization remains a difficult task. This is especially true in case of larger polyatomic molecules where *ab initio* methods are lagging behind experiment.

The computation of photoionization observables relies on transition dipole matrix elements, \mathbf{d}_{fi} , between an initial bound state Φ_i^N and a final continuum state $\Psi_f^{(-)}$ (Harvey *et al* 2014).

$$\mathbf{d}_{fi}(\mathbf{k}_f) = \langle \Psi_{f,\mathbf{k}_f}^{(-)} | \mathbf{d} | \Phi_i^N \rangle, \quad (1)$$

where \mathbf{d} is the dipole operator and \mathbf{k}_f is the momentum of the photoelectron. In principle, whilst obtaining accurate bound wavefunctions Φ_i^N can still be challenging, a wide range of existing quantum chemistry techniques can be used to generate them. The real difficulty lies in the representation of the final continuum state $\Psi_f^{(-)}$. The final wavefunction is comprised of an ion-like component, which represents some final

* Author to whom any correspondence should be addressed.

asymptotic state of the ionized molecule, coupled to the ejected photoelectron. One of the first challenges is to ensure an accurate representation of the oscillating continuum wavefunction. Secondly, at low to intermediate photon-energies (e.g., below 20 eV) there can be several ionic states that have significant contribution to the total photoionization cross-section. Accurate treatment of coupling between excited ionic states typically requires sophisticated close-coupling (CC) calculations. Not only are CC calculations computationally expensive but they also require careful and non-trivial balancing of ionic and neutral state descriptions in order to produce accurate results. The same difficulty applies in the case of electron scattering with molecules.

In this work we focus on the construction of CC models in molecular R-matrix calculations. The R-matrix method is an *ab initio* method for solving the Schrödinger equation which has been implemented for electron scattering and photoionization of poly-atomic molecules in the UKRMol suite of codes. The most recent version of the molecular R-matrix codes, UKRMol+ (Mašín *et al* 2020), has undergone significant re-design and modernization. Some of the most notable improvements include increased parallelization, which has made possible the study of larger molecules, and an interface with a new integrals library (GBTOLib) that is capable of using an arbitrary mixture of B-splines and Gaussian functions to represent the continuum. The mixed continuum is particularly useful for studying larger systems as it reduces the computational demand.

The photoionization capability of UKRMol+ was developed by Harvey *et al* (2014). Following those pioneering developments the method has been applied to photoionization of small molecules (Brigg *et al* 2015, Brambila *et al* 2015, Mašín *et al* 2018, Modak and Antony 2019, Benda *et al* 2020, Benda and Mašín 2021, Wang *et al* 2021).

At the core of the UKRMol+ R-matrix method lies the CC expansion which is used to describe the N -electron photoionization wavefunction, where N is the total number of electrons. The N -electron wavefunction is flexible by design and can be constructed with a variety of different models, such as, static exchange (SE), static exchange plus polarization (SEP) and CC, listed in order of sophistication (see Mašín *et al* (2020) and Tennyson (2010) for more details). Each model has its own strengths and weaknesses, as will be discussed in section 2 but generally speaking the model complexity is proportional to the accuracy of the calculation. For electron scattering calculations, the former statement is largely true (Tennyson 2010), however for photoionization of neutral molecules we have found that this is not the case. Specifically, the SEP model which is typically used to improve upon simple SE calculations actually performs significantly worse for photoionization calculations. This is due to a large amount of spurious resonances and autoionization resonances which occur in the lower-energy region. For electron–molecule scattering the spurious resonances are also present above the threshold for electronic excitation (Morgan *et al* 1997, Tennyson 2010) however, they are usually less severe. This is because, for neutral molecules, photoionization leads to a strong Coulomb

interaction between the ion and the electron which is not present in electron scattering from neutral molecules. Therefore the SEP model is suitable for computation of low-energy elastic scattering data for neutral molecules.

To address the deficiencies of the SEP model for photoionization, we propose a new photoionization model, polarization-consistent coupled Hartree–Fock (PC-CHF). This model eliminates the spurious resonances of the SEP model by explicitly coupling all of the polarization configurations to their corresponding final ionic states.

2. Theory

The general formalism of the R-matrix method has been described in great detail in previous publications, for example, see Tennyson (2010) and Burke (2011). Therefore only a brief overview of the key concepts will be presented here.

In the R-matrix method configuration space is divided into two regions, inner and outer, divided by the R-matrix sphere. The two regions are solved in different ways but the solutions match at the boundary via the R-matrix. The size of the R-matrix sphere must be large enough to contain the charge density of the target because in the outer region the photoelectron must be distinguishable. In practice, this means that the amplitude of all target basis functions must be negligible on the boundary. As mentioned earlier, one of the central pillars of the R-matrix method is the CC expansion used to describe the N -electron wavefunction, ψ_k^N (Burke 2011).

$$\psi_k^N = \mathcal{A} \sum_{ij} c_{ijk} \phi_i^{N-1}(\mathbf{x}_1, \dots, \mathbf{x}_{N-1}) \eta_{ij}(\mathbf{x}_N) + \sum_m b_{mk} \chi_m^N(\mathbf{x}_1, \dots, \mathbf{x}_N). \quad (2)$$

The first term on the right-hand side consists of ionic wavefunctions, $\phi_i^{N-1}(\mathbf{x}_1, \dots, \mathbf{x}_{N-1})$, coupled to continuum orbitals, $\eta_{ij}(\mathbf{x}_N)$ which have a non-zero amplitude on the R-matrix boundary. The second term of equation (2) contains L^2 configurations. These are generated by placing the photoelectron into unoccupied target orbitals (virtual orbitals). The operator \mathcal{A} ensures that the total wavefunction is antisymmetric with respect to exchange of any pair of electrons. Lastly, b_{mk} and c_{ijk} are the coefficients obtained by diagonalising the inner region Hamiltonian (Burke 2011).

2.1. Photoionization models

The key aspect of R-matrix models is the choice of configurations used for construction of the R-matrix states ψ_k^N from equation (2). While the UKRMol+ codes allow for a flexible specification of configurations, only a few standard models are typically used (Mašín *et al* 2020).

Static Exchange (SE) calculations are conceptually the simplest as they include only a single electronic channel. The corresponding electronic state is described on a Hartree–Fock (HF) level. For a closed-shell, neutral molecule with N electrons the following configurations are included:

$$\begin{aligned}
 &(\text{HF})^{N-1}(\text{cont})^1, \\
 &(\text{HF})^{N-1}(\text{virt})^1, \\
 &(\text{HF})^N,
 \end{aligned}
 \tag{3}$$

where the configuration $(\text{HF})^{N-1}$ is obtained from the HF wavefunction $(\text{HF})^N$ by removing one electron from one of the occupied orbitals. The first type of configuration corresponds to an HF-like state coupled to the continuum orbital. The second type corresponds to the photoelectron occupying a virtual orbital. The final type of configuration is simply the HF wavefunction of the neutral molecule.

Static Exchange plus Polarization (SEP) is the natural extension to SE. In addition to the three types of configuration listed in equation (3), SEP allows single excitation of the target into a set of virtual orbitals, to model the effect of polarization by the photoelectron. This is represented as,

$$(\text{core})^{N_c}(\text{valence})^{N_v-2}(\text{virt})^2,
 \tag{4}$$

where N_c is the number of core (frozen) electrons, N_v is the number of valence electrons and $N_c + N_v = N$. The amount of polarization can be tuned by including more virtual orbitals and by increasing the number of valence electrons which can partake in single excitations N_v .

As is the case for the SE model, the calculation still features only a single ionic state. Therefore the additional polarization configurations are only coupled to one final ionic state. For electron scattering calculations SEP has proved to be an accurate model for computing cross sections and for the characterization of low-lying shape resonances. However, for photoionization the absence of coupling the polarization configurations to other energetically-accessible excited states causes the model to give strongly distorted and inaccurate results. This is demonstrated in figure 1 showing a comparison of the SEP results for photoionization of water with an SE calculation and experimental data. Note that the SEP model performs significantly worse than the simpler SE model. In this example, the SEP model consisted of $N_c = 4$ core electrons, $N_v = 6$ valence electrons and $n_{\text{vir}} = 14$ virtual orbitals. The SE model also uses $n_{\text{vir}} = 14$ virtual orbitals. For both calculations the atomic basis cc-pVTZ was used with a mixed B-spline and Gaussian continuum.

Close-Coupling (CC) is the most sophisticated model. Typically, a complete active space self-consistent field (CASSCF) description of the target is used in conjunction with a multi-channel CC scattering model. The CC model consists of configurations of the following types,

$$\begin{aligned}
 &(\text{core})^{N_c}(\text{CAS})^{N_a-1}(\text{cont})^1, \\
 &(\text{core})^{N_c}(\text{CAS})^{N_a}, \\
 &(\text{core})^{N_c}(\text{CAS})^{N_a-1}(\text{virt})^1, \\
 &(\text{core})^{N_c}(\text{CAS})^{N_a-2}(\text{virt})^2,
 \end{aligned}
 \tag{5}$$

where N_a is the number of electrons in the CASSCF active space and $N_c + N_a = N$. The configurations here are an

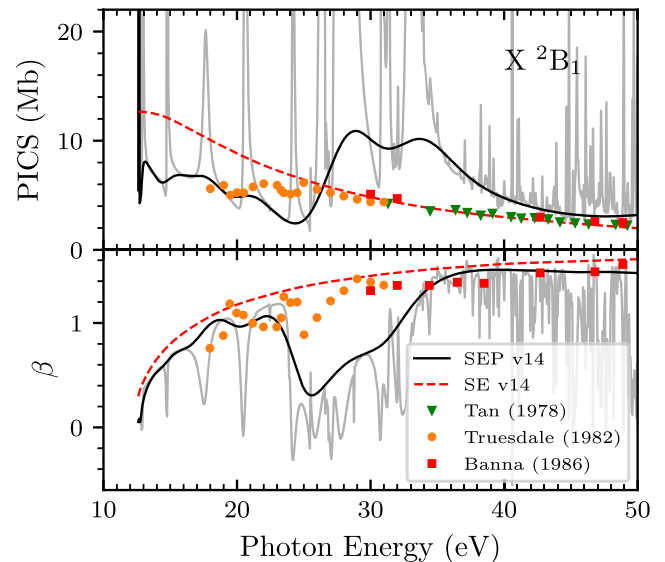


Figure 1. H_2O photoionization cross-section (top) and asymmetry parameter (bottom) for transition into the ground ionic state X^2B_1 . Smoothed (black solid) and raw (light grey) R-matrix calculation using the SEP model compared with SE results (red dashed) and the experimental data of Tan *et al* (1978) (green triangle), Truesdale *et al* (1982) (orange circle) and Banna *et al* (1986) (red square).

extension of those for SEP and SE except now the target description is no longer a single HF-like state: multiple ionic states described on multi-configurational level are now included in equation (2). Therefore the L^2 -configurations, listed on the last three lines of equation (5), can now couple to all of the included final ionic states. The configurations $(\text{core})^{N_c}(\text{CAS})^{N_a-1}$ from the first line of equation (5) are contracted with the ionic CAS wavefunctions to reduce the size of the Hamiltonian matrix. At the same time this contraction implies a change of ionic basis from individual configurations to ionic eigenstates. The last set of configurations, which place two electrons into the virtual orbitals, provide additional polarization description but these are typically not needed.

Polarization-Consistent Coupled Hartree-Fock (PC-CHF) is a new model and the focus of this work. It is designed to sit, conceptually, between the SEP and CC scattering models. The PC-CHF model is designed to eliminate some of the deficiencies of the SEP model whilst retaining the physically simpler picture of HF-like ionic states. This approach can be advantageous in many cases since the HF description of ionic states is appropriate for many valence molecular states and is easy to construct as opposed to CASSCF wavefunctions. For CASSCF calculations one often requires non-trivial quantum chemistry experience in order to select appropriate model parameters.

This new model uses the same L^2 configurations as the SEP model but uses a larger number of ionic states which are determined unambiguously and consistently with the set of L^2 configurations. The PC-CHF model can be described by the following set of configurations

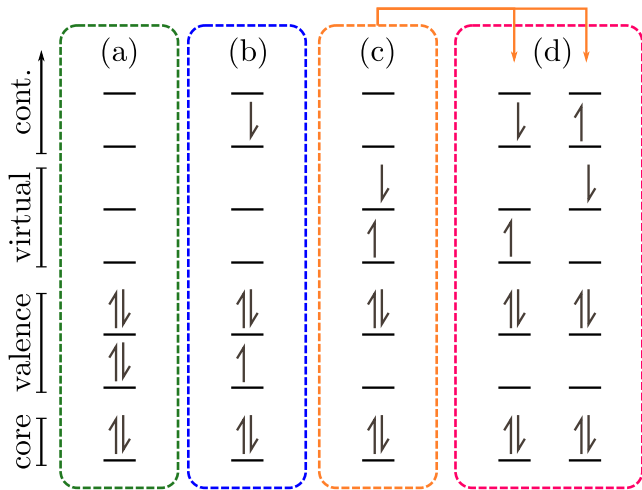


Figure 2. Schematic diagram of the different types of configuration used in the PC-CHF model (see text for more details).

$$\begin{aligned}
 & (\text{HF})^{N_c}, \\
 & (\text{core})^{N_c}(\text{valence})^{N_v-1}(\text{cont})^1, \\
 & (\text{core})^{N_c}(\text{valence})^{N_v-2}(\text{virt})^2, \\
 & (\text{core})^{N_c}(\text{valence})^{N_v-2}(\text{virtual})^1(\text{cont})^1, \\
 & (\text{core})^{N_c}(\text{valence})^{N_v-1}(\text{virtual})^1,
 \end{aligned} \tag{6}$$

where N_v and N_c are the same quantities as before. The first configuration from equation (6) is the HF wavefunction of the initial state which is shown schematically in figure 2(a). The second type of configurations correspond to HF-like ionic wavefunctions with the photoelectron in a continuum orbital (figure 2(b)). The third type of configurations are the polarization configurations of the SEP model (figure 2(c)). The fourth set of configurations are generated by considering the polarization configurations. We can see that two distinct ionic states are implied by the specific polarization configuration shown in figure 2(c). An example configuration for each distinct final ionic state is shown in figure 2(d). The unique set of all such HF-like ionic states is then included in the CC expansion, equation (2). The final set of configurations are similar to those described for the SE model in equation (3) where one electron is placed into the virtual orbitals.

This is why we describe the calculation as polarization-consistent: the choice of the SEP polarization configurations uniquely determines the number and type of ionic states to be generated and included in the calculation.

The number of ionic states generated, N_{states} , is determined by the number of valence orbitals, n_{val} , and the number of virtual orbitals, n_{vir} , by accounting for all unique and symmetry-allowed combinations

$$N_{\text{states}} \geq n_{\text{val}} + \frac{n_{\text{val}}(n_{\text{val}} + 1)}{2} n_{\text{vir}}. \tag{7}$$

As illustrated in figure 3, the actual number of states generated can be greater than the number of unique combinations of target orbitals due to the spin degrees of freedom: for a given set

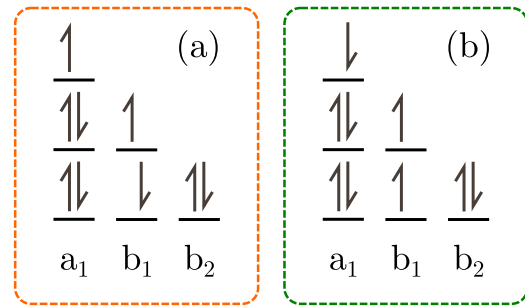


Figure 3. Schematic diagram of two determinants for H_2O^+ which differ only by spin flips of the unpaired electrons. Determinants (a) and (b) have the same total spin-space symmetry i.e., 2A_1 . The diagrams show the occupation of the target orbitals in each symmetry.

of occupied orbitals two spin-adapted states may be generated in certain cases.

3. Results

In this section we will discuss the results obtained using the new photoionization model, PC-CHF. The PC-CHF model is applied to three molecular targets: H_2O , N_2O and formic acid (HCOOH) and the data are compared against existing theory and experimental measurements where available.

We present raw and smoothed data obtained using the PC-CHF model. The smoothing algorithm is explained in a previous publication (Benda *et al* 2020) but essentially the partial-wave dipoles are convoluted with a Gaussian with a variable width dependent on the photoelectron kinetic energy. This is to remove very narrow spikes in the observables that ultimately will not be resolved in the experiment. Note that it is the partial-wave dipoles that are smoothed and not the observables themselves.

For both the PC-CHF and CC calculations we shift the first ionization threshold to match experimental data—excited ionic states are shifted by this same difference. The shift occurs prior to the evaluation of the cross-sections and asymmetry parameters. SE calculations only contain a single ionic state and therefore each threshold is shifted individually to the corresponding experimental data. The photoionization cross-sections and asymmetry parameters produced in this work are provided as supplementary data, which can be found online at (<https://stacks.iop.org/JPB/55/035201/mmedia>).

3.1. Photoionization of H_2O

PC-CHF calculations for H_2O were carried out using the equilibrium geometry of the neutral molecule i.e., $r(\text{OH}) = 0.958 \text{ \AA}$ and $\angle(\text{OHO}) = 104.5^\circ$ (Hoy and Bunker 1979). The Psi4 quantum chemistry program (Smith *et al* 2020) was used to generate HF orbitals in the cc-pVTZ basis. The effect of using HF orbitals optimized for the ground state of the neutral molecule, H_2O , and the ground state of its ion, H_2O^+ , are investigated—PC-CHF(N) and PC-CHF(I), respectively. Photoionization observables depend on the initial neutral and final ionic wavefunctions. Choosing HF orbitals

Table 1. H₂O ionization thresholds, I_p , for the first three ionic states. Energies computed with the PC-CHF model using HF orbitals optimized for the neutral molecule, H₂O (N), and the ion, H₂O⁺ (I), are compared with the calculations of Benda *et al* (2020) and the experimental data of Brundle and Turner (1968) and Potts and Price (1972). Energies obtained by shifting the first ionization threshold to that of experiment are shown in parentheses.

State	I_p (eV)				
	PC-CHF(N)	PC-CHF(I)	CC ^a	Ref. 1 ^b	Ref. 2 ^c
X ² B ₁	17.39 (12.60)	14.34 (12.60)	12.82 (12.60)	12.61	12.6
A ² A ₁	19.38 (14.59)	16.87 (15.13)	15.18 (14.96)	14.74	14.7
B ² B ₂	22.97 (18.18)	21.18 (19.44)	19.35 (19.13)	18.55	18.5

^aBenda *et al* (2020).

^bBrundle and Turner (1968).

^cPotts and Price (1972).

optimized for the neutral typically improves the description of the initial wavefunction at the expense of the final wavefunction description. This is a balancing act and the best choice will depend on the target molecule.

Ionization thresholds for the first three ionic states are shown in table 1. For the PC-CHF model we use a simplistic HF-like description of the target states. Therefore, the ionic state energies cannot be expected to be as accurate as those obtained from more sophisticated CASSCF calculations, for example, those obtained by Benda *et al* (2020). However, in this work, and that of Benda *et al* (2020), the first ionization threshold is shifted to match the experimental value of 12.6 eV. Once shifted, the relative excitation thresholds between the ionic states obtained in the PC-CHF model, for both the neutral molecule and the ion, are much closer to those from the experiment (Potts and Price 1972) and CC theory (Benda *et al* 2020). The unaltered energies from the PC-CHF(I) model, however, are much better than those from the PC-CHF(N) model. This is to be expected as the HF orbitals are optimized for the ion and therefore they provide a better description of the ionic states.

For both PC-CHF models we used $n_{\text{val}} = 3$ valence orbitals and $n_{\text{vir}} = 14$ virtual orbitals which gives rise to 129 unique ionic states. For the continuum a mixed Gaussian type orbital (GTO) and B-spline type orbital (BTO) basis was used with angular momentum $\ell = 0, \dots, 5$. The GTO exponents were optimized for radius of $r = 10$ a.u. and a partially overlapping BTO basis was included starting from $r = 8$ a.u. to the R-matrix radius $r = 15$ a.u.. For each BTO partial wave we used a radial basis set consisting of 14 B-splines of order 6. For symmetric orthogonalization of the continuum we used a deletion threshold of 1.0×10^{-7} .

The CC calculation of Benda *et al* (2020) uses HF orbitals optimized for the ionized molecule, H₂O⁺ and the same atomic basis as used in our PC-CHF calculations, cc-pVTZ. In their work they use two models, one smaller and one larger. The larger model has been used for the comparisons in this work. Their large model consisted of a CASSCF model with 1 frozen orbital and 14 active orbitals i.e., CAS (7, 14). The R-matrix radius was the same as that used in this work, $a = 15$ a.u.. The continuum basis consisted of 30 B-splines of order 6 and the highest partial wave included was $\ell_{\text{max}} = 6$, although the authors note that convergence was

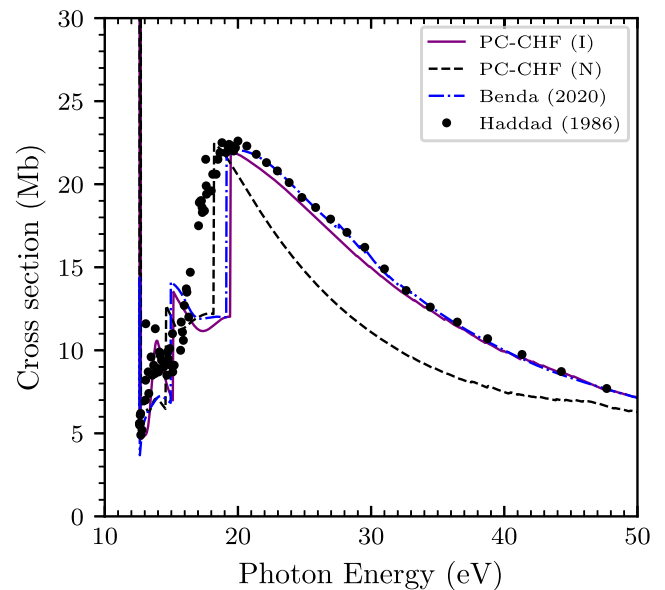


Figure 4. H₂O total photoionization cross-section. Data from the PC-CHF(I) (purple solid) and PC-CHF(N) (black dashed) models are compared with the CC results of Benda *et al* (2020) (blue dot-dash) and the experimental data of Haddad and Samson (1986) (black circle).

obtained for $\ell_{\text{max}} = 4$. Their scattering model included 50 ionic states.

In the total photoionization cross-section for water, shown in figure 4, there are three mainline transitions that correspond to ionization from the three outer valence orbitals, leading to the final ionic states X ²B₁, A ²A₁ and B ²B₂. In this figure, we compare the total photoionization cross section calculated with the PC-CHF model with the experimental measurements of Haddad and Samson (1986) and the CC calculations of Benda *et al* (2020). Across the energy range considered in this work we find excellent agreement between PC-CHF(I) calculations, previous calculations and experimental data. However, the PC-CHF(N) model, which employed HF orbitals of the neutral molecule, under-estimates the total photoionization cross-section in the 20 eV to 50 eV energy region. In fact, as we will see in the state-resolved cross-sections, figure 5, the PC-CHF(N) model consistently under-estimates the partial cross-sections also. We believe that this is related to the

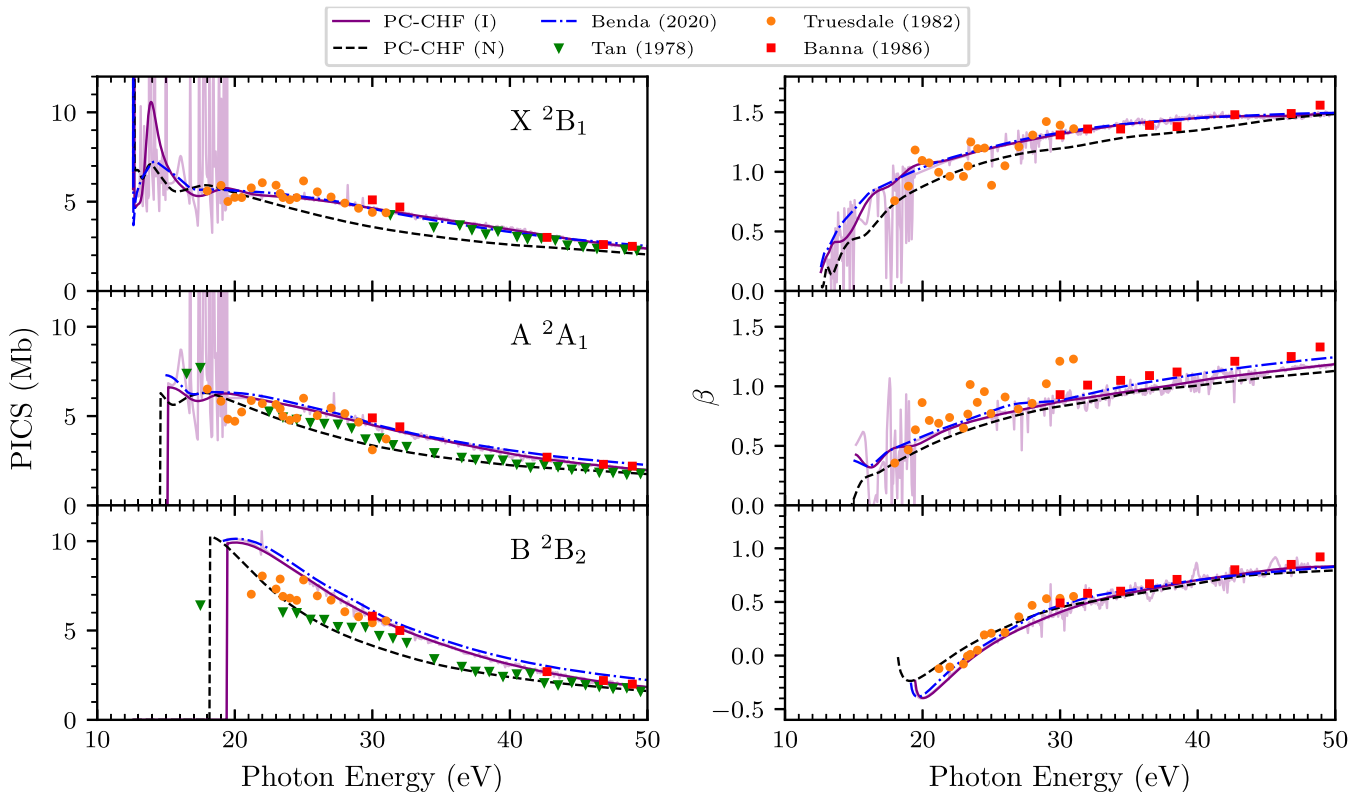


Figure 5. H₂O photoionization cross-section (left panels) and asymmetry parameters (right panels) for transitions into the first three ionic states, X ²B₁, A ²A₁ and B ²B₂. The smoothed (purple solid) and raw (light purple) results of the PC-CHF(I) model are compared with the PC-CHF(N) model (black dashed), CC results of Benda *et al* (2020) (blue dot-dash) and the experimental data of Tan *et al* (1978) (green triangle), Truesdale *et al* (1982) (orange circle) and Banna *et al* (1986) (red square).

importance of orbital relaxation immediately following ionization of the molecule.

In figure 5 cross sections and asymmetry parameters, β , calculated with the PC-CHF model are compared against CC calculations of Benda *et al* (2020) and the experimental measurements of Tan *et al* (1978), Truesdale *et al* (1982) and Banna *et al* (1986). For all of the final ionic states shown in figure 5, X ²B₁, A ²A₁ and B ²B₂ the agreement between the PC-CHF(I) model and the accurate CC calculations of Benda *et al* (2020) is excellent. Some discrepancies close to the ionization threshold are present in the cross-section and asymmetry parameter for the X ²B₁ state but these are to be expected due to the presence of large groups of closely spaced autoionizing resonances. Compared to the PC-CHF(I) and CC models, the data from the PC-CHF(N) model under-estimate the partial cross-sections for all three final ionic states. Despite this, the asymmetry parameters between the two PC-CHF models are roughly unaffected by the choice of HF orbitals.

For the ground ionic state, X ²B₁, the experimental measurements of Tan *et al* (1978), Truesdale *et al* (1982) and Banna *et al* (1986) are in close agreement and they show a preference for the PC-CHF(I) and CC models, as opposed to the PC-CHF(N) model. However for the excited ionic states, A ²A₁ and B ²B₂, there is less agreement between the three experiments. When comparing against the experimental data of Tan *et al* (1978) the PC-CHF(N) model has the best agreement, but, when comparing to the two newer experiments of Truesdale

et al (1982) and Banna *et al* (1986) the CC and PC-CHF(I) models have the closest agreement. Based on the agreement in the total cross-section (figure 4) and with the accurate CC model of Benda *et al* (2020) we believe the PC-CHF(I) model is more appropriate than the PC-CHF(N) model.

3.2. Photoionization of N₂O

In this section the PC-CHF model is applied to N₂O in order to explore the validity of this approach on a more complex molecule. Whilst still a triatomic molecule, N₂O presents several new challenges. Firstly, it has 22 electrons, which is more than double the number in H₂O. Secondly, unlike H₂O, N₂O is a linear molecule belonging to the point group C_{∞v}. The UKRMol+ code only supports Abelian point group symmetries and therefore we have to use a lower symmetry group C_{2v}. In C_{2v}, the Π states are represented by degenerate states of symmetry B₁ and B₂ and both symmetries have to be included in our calculation.

The degeneracy introduced by the lower symmetry point group C_{2v} creates an additional computational problem. Currently, the UKRMol+ code is not structured to handle degenerate states that share identical properties but from different configuration state functions (CSFs). For example, this situation arises when the totally symmetric ionic core is described by a CSF containing double occupation of two degenerate orbitals of different symmetry. To get around this problem we combine the set of PC-CHF ionic configurations which share

the same symmetry as a multi-configurational basis for the ionic wavefunctions, ϕ_i^{N-1} , from equation (2). This effectively produces a configuration interaction description of the ionic states but where the configurations have been automatically selected according to the PC-CHF model. For the two molecules where we could run both types of model, H₂O and HCOOH, we tested the effect of the ionic configuration interaction (not shown) and it made minimal difference to the final results. The biggest difference is a small change in the ionic state thresholds. That is, in this version of the PC-CHF model the target state description depends on the size of the model i.e., on the choice of n_{val} and n_{vir} .

For N₂O we use Psi4 with the cc-pVDZ atomic basis set to compute HF orbitals optimized for the neutral molecule. We use the equilibrium geometry, $r(\text{NN}) = 1.128 \text{ \AA}$ and $r(\text{NO}) = 1.184 \text{ \AA}$ (Herzberg 1966). PC-CHF(N) calculations were also performed using the cc-pVTZ basis set (not shown) but the change of atomic basis made negligible difference.

To compute photoionization observables for the first four ionic states of N₂O a PC-CHF(N) model with $n_{\text{val}} = 6$ valence orbitals was required. This is due to the splitting of the two Π states in C_{2v} symmetry. Sufficient convergence of the PC-CHF(N) model is obtained using $n_{\text{vir}} = 8$ virtual orbitals. The specified valence and virtual orbitals imply a total of 230 unique ionic states. For the continuum we used the same mixed GTO/BTO-type basis as for our water calculations, see above, except for N₂O a maximum partial wave of $\ell_{\text{max}} = 6$ was required for convergence of the photoionization observables. PC-CHF(I) calculations using the HF orbitals optimized for the ion were also carried out (not shown). Unlike H₂O, there was a negligible difference between the two sets of HF orbitals. Therefore we selected the HF orbitals optimized for the neutral molecule, PC-CHF(N).

Four SE calculations were performed for comparison with the PC-CHF(N) and CC models, one for each of the ionic target states: X ²Π, A ²Σ⁺, B ²Π and C ²Σ⁺. We use the same geometry, atomic basis set and continuum basis as for the PC-CHF(N) calculations. In all cases the SE calculations used $n_{\text{vir}} = 8$ virtual orbitals.

The CC calculation of Benda *et al* (2022) uses the cc-pVTZ atomic basis set. For the continuum a BTO only basis set was used consisting of 30 B-splines. This calculation uses the same R-matrix radius, $a = 15 \text{ a.u.}$, as our N₂O calculations. The ionic wavefunctions are described by a CASSCF model with 3 frozen orbitals and 11 active orbitals i.e., CAS (15, 11) and 7 virtual orbitals are added to account for additional polarization of the molecule. The scattering calculation includes 200 ionic states.

The ionization thresholds obtained with the PC-CHF(N) model are shown in table 2. Comparing the unaltered thresholds with the accurate CC calculations of Benda *et al* (2022) we can see that the HF description is relatively poor. However, once we shift the first ionization potential to the experimental value we can see better agreement between the thresholds obtained from the PC-CHF(N) and CC calculations and the experimental data of Truesdale *et al* (1983). Each of the four SE thresholds are obtained from independent SE calculations and they are all shifted separately to match

Table 2. N₂O ionization thresholds, I_p , for the first four ionic states. Energies computed with the PC-CHF(N) model are compared with SE calculations, the CC calculations of Benda *et al* (2022) and the experimental data of Truesdale *et al* (1983). Energies obtained by shifting the first ionization threshold to that of experiment are shown in parentheses.

State	I_p (eV)			Ref. 1 ^b
	SE	PC-CHF(N)	CC ^a	
X ² Π	13.44 (12.89)	18.66 (12.89)	13.66 (12.89)	12.9
A ² Σ ⁺	18.94 (16.39)	22.83 (17.06)	17.18 (16.41)	16.4
B ² Π	20.86 (18.30)	24.50 (18.72)	19.33 (18.56)	18.3
C ² Σ ⁺	22.59 (20.10)	26.54 (20.77)	21.31 (20.54)	20.1

^aBenda *et al* (2022).

^bTruesdale *et al* (1983).

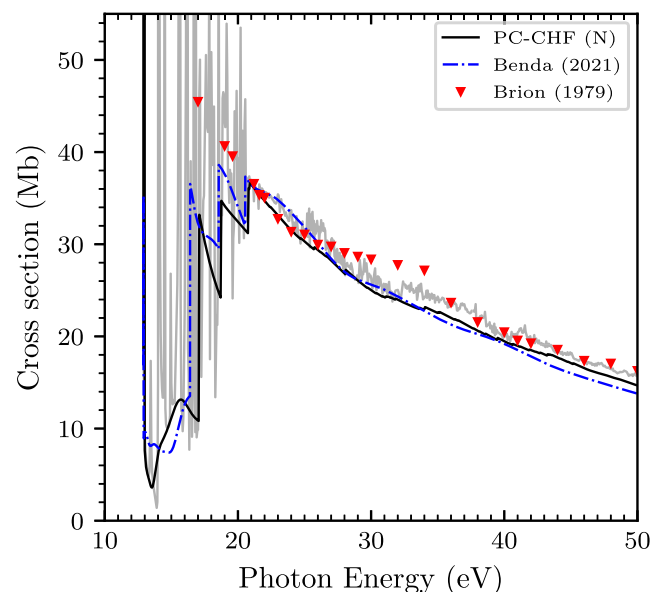


Figure 6. N₂O total photoionization cross-section. The smoothed (black solid) and raw (light grey) data from the PC-CHF(N) model are compared with the CC results of Benda *et al* (2022) (blue dot-dash) and the experimental data of Brion and Tan (1979) (red triangle).

thresholds from experiment. Note that the unaltered thresholds for the SE model appear better than the PC-CHF model. The thresholds depend on the difference between the ionic states and the neutral ground state. In PC-CHF the neutral ground state is significantly improved whilst both models share the same ionic state description.

Figure 6 shows the total photoionization cross-section for N₂O. Across the energy range considered, there is good agreement between the PC-CHF(N) calculation and the CC model of (Benda *et al* 2022). Furthermore, both theories are in good agreement with the experimental results of (Brion and Tan 1979). Below 20 eV there are differences between the two theories and the experiment but this is due to large numbers of tightly packed resonances, which are not resolved by the experiment. Around 30 eV the experimental data seem to indi-

cate the presence of a broad peak but this is not observed in either of the two theoretical calculations.

Figure 7 shows the state-resolved cross-sections and asymmetry parameters for the first four ionic states of N_2O i.e., $X^2\Pi$, $A^2\Sigma^+$, $B^2\Pi$ and $C^2\Sigma^+$. The two calculations, PC-CHF(N) and CC, show generally good agreement in the photoionization cross-sections. The biggest difference occurs in the $C^2\Sigma^+$ state close to threshold where the CC calculation has a larger cross-section around 22 eV than the PC-CHF(N) model. The SE model for the $X^2\Pi$ state is significantly over-estimating the cross-section at lower photon energies i.e., below 30 eV. This deficiency is removed in the PC-CHF model and is thus clearly caused by the absence of coupling to other ionic states. The SE cross-section data for the $A^2\Sigma^+$, $B^2\Pi$ and $C^2\Sigma^+$ states, however, are in closer agreement with the CC and PC-CHF(N) models.

We now compare the asymmetry parameters in figure 7. The two Π states, $X^2\Pi$ and $B^2\Pi$, show good agreement between the two models, CC and PC-CHF, and good agreement with the experimental measurements. However, it appears that the asymmetry parameters for the first two Σ states, $A^2\Sigma^+$ and $C^2\Sigma^+$, are more sensitive to the choice of model. For the $A^2\Sigma^+$ state the PC-CHF and CC models show substantial differences in the mid-range of photon energies i.e., from threshold to 40 eV. For the $C^2\Sigma^+$ there is qualitative agreement between the PC-CHF and CC models across the energy range considered. However, below 40 eV photon energy the two calculations are not in agreement. For the $A^2\Sigma^+$ state, the experimental data appear to favour the CC model, however, in the $C^2\Sigma^+$ state asymmetry parameter it is not clear which theory is better.

The differences between the calculations in the state-resolved photoionization cross-sections and asymmetry parameters show just how challenging it can be to model photoionization. It would appear that for accurate photoionization data we need accurate wavefunctions and careful treatment of coupling between the different channels. For the simple SE model, we can see that the cross-section and the asymmetry parameter for the $A^2\Sigma^+$ state are in reasonable agreement with experiment and the sophisticated CC calculations. However, when we add multiple scattering channels with the PC-CHF(N) model the asymmetry parameter deteriorates, even though we keep a similar, if not better, description of the ionic and neutral wavefunctions. This discrepancy is possibly due to inaccurate values of the transition moments that come into play in strongly dipole-coupled transitions or due to lack of inclusion of important multiply-excited states.

Braunstein and McKoy (1987) identified two shape resonances, at roughly 20 eV and 40 eV, affecting the photoionization cross-section and asymmetry parameter for the $A^2\Sigma^+$ state. The first resonance occurs near threshold and is responsible for the initial peak in the cross-section. The second resonance was not visible in the cross-section but was attributed to the broad dip in the asymmetry parameter in the energy region 30–40 eV. These resonances may play a role in the discrepancy between the PC-CHF and CC results.

3.3. Photoionization of formic acid

Formic acid, HCOOH , is the simplest carboxylic acid and it has two sites which can support hydrogen bonds. This makes it an ideal candidate to study biomolecules such as amino acids and DNA base pairs (Tenorio *et al* 2019). In this work we will only focus on the monomer for which prior theoretical and experimental data are available (Leach *et al* 2002, Schwell *et al* 2002, Fujimoto *et al* 2020).

Formic acid is a planar molecule which exists as two isomers, *cis*- HCOOH and *trans*- HCOOH , see figure 8. The most stable isomer is that of *trans*- HCOOH with a barrier height of roughly 5 kcal mol⁻¹ (0.22 eV) (Goddard *et al* 1992). At room temperature the Boltzmann distribution law implies that the abundance of the *cis* conformer is negligible (Takeshita 1995) and hence the photoelectron spectra will largely be dominated by the *trans* conformer. Therefore we only consider *trans*- HCOOH in this work.

We have performed R-matrix calculations using three different models, SE, PC-CHF(N) and CC. All three models use the same atomic basis, cc-pVDZ. For the SE and PC-CHF(N) models the equilibrium geometry was taken from the experimental measurements of Herzberg (1966). However, for the CC calculations we used Molpro (Werner *et al* 2012) to optimize the geometry for the cc-pVDZ basis set. This was found to improve the agreement of the ionization thresholds with the reference data of Schwell *et al* (2001), Leach *et al* (2002) and Brundle *et al* (1969) (see table 3).

The SE and PC-CHF(N) models use HF orbitals, generated using Molpro, optimized for the neutral molecule. The dominant contributions to the total photoionization cross-section come from transitions into the first six ionic states, which correspond to ionization of the six outermost valence orbitals, as listed in table 3. Therefore, for our PC-CHF(N) model we use $n_{\text{val}} = 6$ valence orbitals. To converge the PC-CHF model we used $n_{\text{vir}} = 7$ virtual orbitals, which generates 258 unique ionic states. For the SE model we use $n_{\text{vir}} = 15$ virtual orbitals.

In the CC calculation the target is described using state-averaged CASSCF orbitals. Seven states are included in the state-averaging procedure; the six mainline transition states and the neutral ground state. The neutral ground state was given a weight of 50% and the ionic states each had equal weight. The active space freezes 12 of the core electrons, which corresponds to freezing the 1s and 2s shells on each of the carbon and oxygen atoms. The remaining 11 electrons occupy 12 a' orbitals and 3 a'' orbitals. This can be summarized as CAS (11, 15). In the CC model we include the lowest 200 ionic states although convergence was obtained around 100 states.

All three models (SE, PC-CHF(N) and CC) use the same mixed GTO/BTO-type continuum as the H_2O calculation.

Fujimoto *et al* (2020) used ePolyScat-D (Gianturco *et al* 1994) to compute state-resolved photoionization cross-sections and asymmetry parameters for the first 6 ionic states of formic acid. The partial cross-sections were then summed to provide the total photoionization cross-section. In figure 9 we compare the total photoionization cross-sections

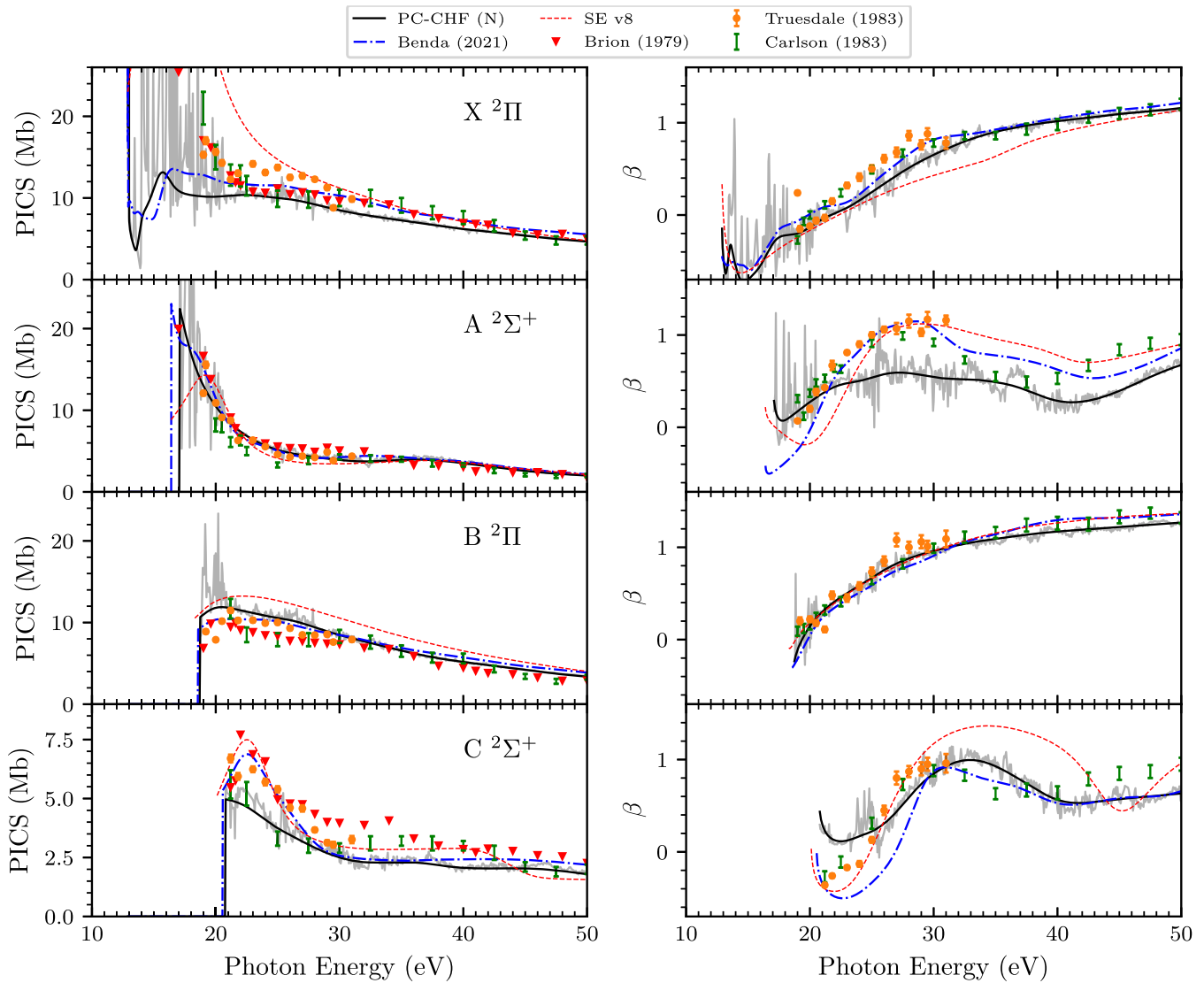


Figure 7. N_2O photoionization cross-section (left panels) and asymmetry parameters (right panels) for transitions into the first four ionic states, $X^2\Pi$, $A^2\Sigma^+$, $B^2\Pi$ and $C^2\Sigma^+$. The smoothed (black solid) and raw (light grey) results of the PC-CHF(N) model are compared with SE (red dashed) calculations, the CC (blue dot-dash) calculations of Benda *et al* (2022) and the experimental data of Brion and Tan (1979) (red triangle), Carlson *et al* (1983) (orange circle) and Truesdale *et al* (1983) (green bar).

obtained using the PC-CHF(N) and CC R-matrix models with the ePolyScat-D calculations of Fujimoto *et al* (2020) and experimental data of Fujimoto *et al* (2020), Leach *et al* (2002) and Schwell *et al* (2002). The photoionization cross-section data Leach–Schwell (2002) is a combination of the photoabsorption cross-section measured by Leach *et al* (2002) and the quantum efficiency measured by Schwell *et al* (2002).

The CC total photoionization cross-section is in good agreement with the experimental data of Leach–Schwell (2002). Although the experimental data only covers the lower energy region i.e., below 23 eV, it appears as though both cross-sections exhibit a plateau starting around 18 eV. This plateau is also observed in the experimental data of Fujimoto *et al* (2020) albeit with a slightly larger cross-section. The PC-CHF(N) model also shows a plateau-like structure at the same energy but with a significantly smaller cross-section. In the calculations of Fujimoto *et al* (2020) the plateau is not observed,

instead the cross-section peaks around 17 eV and then falls off as the photon energy increases. The ePolyScat-D data of Fujimoto *et al* (2020) is based on a single-active electron model which omits state-coupling and hence models elastic collisions only. Therefore, we suspect that it may over estimate the partial, and hence, total cross-sections. This will be discussed further when we compare the state-resolved cross-sections.

Figure 10 compares the state-resolved R-matrix photoionization cross-sections and asymmetry parameters with the ePolyScat-D calculations of Fujimoto *et al* (2020). In general, for the first 6 ionic states, we can see close agreement between the SE calculation using the R-matrix method and the calculation from Fujimoto *et al* (2020). This is to be expected as both calculations contain only a single elastic channel. The biggest difference occurs in the cross-section and asymmetry parameter for the state $8a'$. This is most likely caused by the effective scattering potential used in the ePolyScat-D

Table 3. Formic acid ionization thresholds, I_p , corresponding to ionization from the six highest occupied molecular orbitals. Energies computed with the SE, PC-CHF and the CC R-matrix models are compared with the calculations of Fujimoto *et al* (2020) and the experimental data of Schwell *et al* (2001), Leach *et al* (2002) and Brundle *et al* (1969). Energies obtained by shifting the first ionization threshold to that of experiment are shown in parentheses.

Orbital	I_p (eV)				
	SE	PC-CHF(N)	CC (200)	Ref. 1 ^{a,b}	Ref. 2 ^c
10 a'	12.78 (11.32)	16.90 (11.32)	12.48 (11.32)	11.33	11.51
2 a''	13.39 (12.38)	17.51 (11.93)	13.61 (12.45)	12.38	12.51
9 a'	16.35 (14.81)	20.50 (14.93)	16.27 (15.11)	14.81	14.74
1 a''	17.26 (15.35)	21.41 (15.84)	17.23 (16.08)	15.35	15.72
8 a'	19.30 (16.97)	23.48 (17.91)	19.29 (18.14)	16.97	17.13
7 a'	19.62 (17.28)	23.82 (18.24)	19.67 (18.51)	17.28	17.70

^aSchwell *et al* (2001).

^bLeach *et al* (2002).

^cBrundle *et al* (1969).

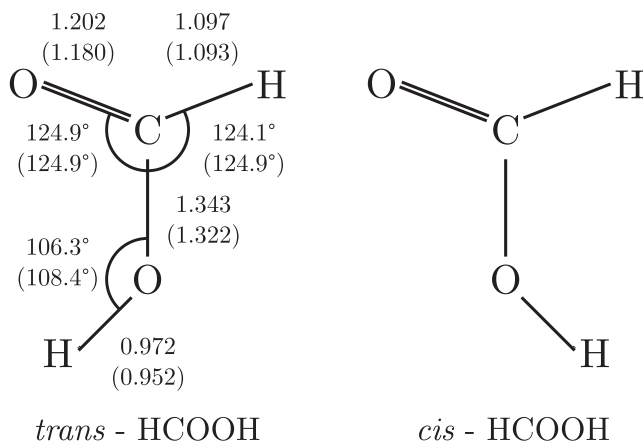


Figure 8. Diagram of the two conformers of HCOOH (*trans*-HCOOH is used in this work). Two geometries are shown, the experimentally derived geometry (Herzberg 1966) and the optimized geometry (shown in parentheses) calculated using Molpro with the cc-pVDZ basis set. Internuclear distances are given in Å.

calculations, which differs from the static potential with exact exchange implied by our SE model.

For the 10 a' state, the cross-section for both SE and ePolyScat-D calculations show a peak around 18 eV. Examination of the eigenphase sums, for the SE calculation, reveals a broad a' shape resonance at 18.6 eV with a width of 4.1 eV. We can see that by adding multi-channel effects, in both the PC-CHF(N) and CC models, the cross-section significantly reduces in the 15 eV to 25 eV region. Neglecting open-channels, as in the SE and ePolyScat-D calculations typically leads to an over-estimation of the photoionization cross-section in the resonance region. A similar effect was observed in CO₂ by Mašín *et al* (2018).

On the whole, there is acceptable agreement between the PC-CHF, CC and ePolyScat-D state-resolved cross-sections e.g., states 2 a'' , 1 a'' and 8 a' . The notable exceptions are for states 9 a' and 7 a' . For the higher excited states it could be that the HF picture of the ion begins to breakdown. In fact, Schirmer *et al* (1978) investigated the quasi-particle nature of ionization in HCOOH, in which main line transitions correspond to ionization of an electron from a single valence

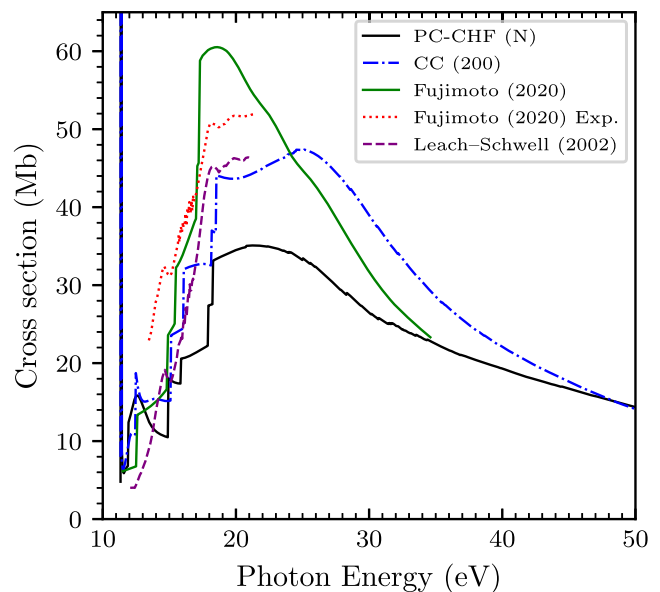


Figure 9. Formic acid total photoionization cross-section. Data from the PC-CHF(N) calculation (black solid) are compared with the CC results (blue dot-dash), the ePolyScat-D calculations of Fujimoto *et al* (2020) (green solid), the experimental measurements of Fujimoto *et al* (2020) (red dotted) and the combined experimental data (Leach–Schwell (2002)—see text for details) from Leach *et al* (2002) and Schwell *et al* (2002) (purple dashed).

orbital. For ionization out of 6 a' the single orbital picture is already completely wrong. Even though it is mostly valid for the first 6 ionic states, there are likely important correlation effects that are not captured in the simpler PC-CHF picture. Therefore it is more likely that the CC results are more accurate.

Comparing the asymmetry parameters, it appears as though all three models (PC-CHF(N), CC and ePolyScat-D) show qualitative agreement for most states. The biggest difference lies in the asymmetry for the 8 a' state. This corresponds to a higher-lying ionic state and therefore this difference is not so surprising. Based on previous arguments it is likely that the CC result is the more accurate one, however, there are no experimental data available for any of the state-resolved observables. Therefore no firm conclusions can be drawn.

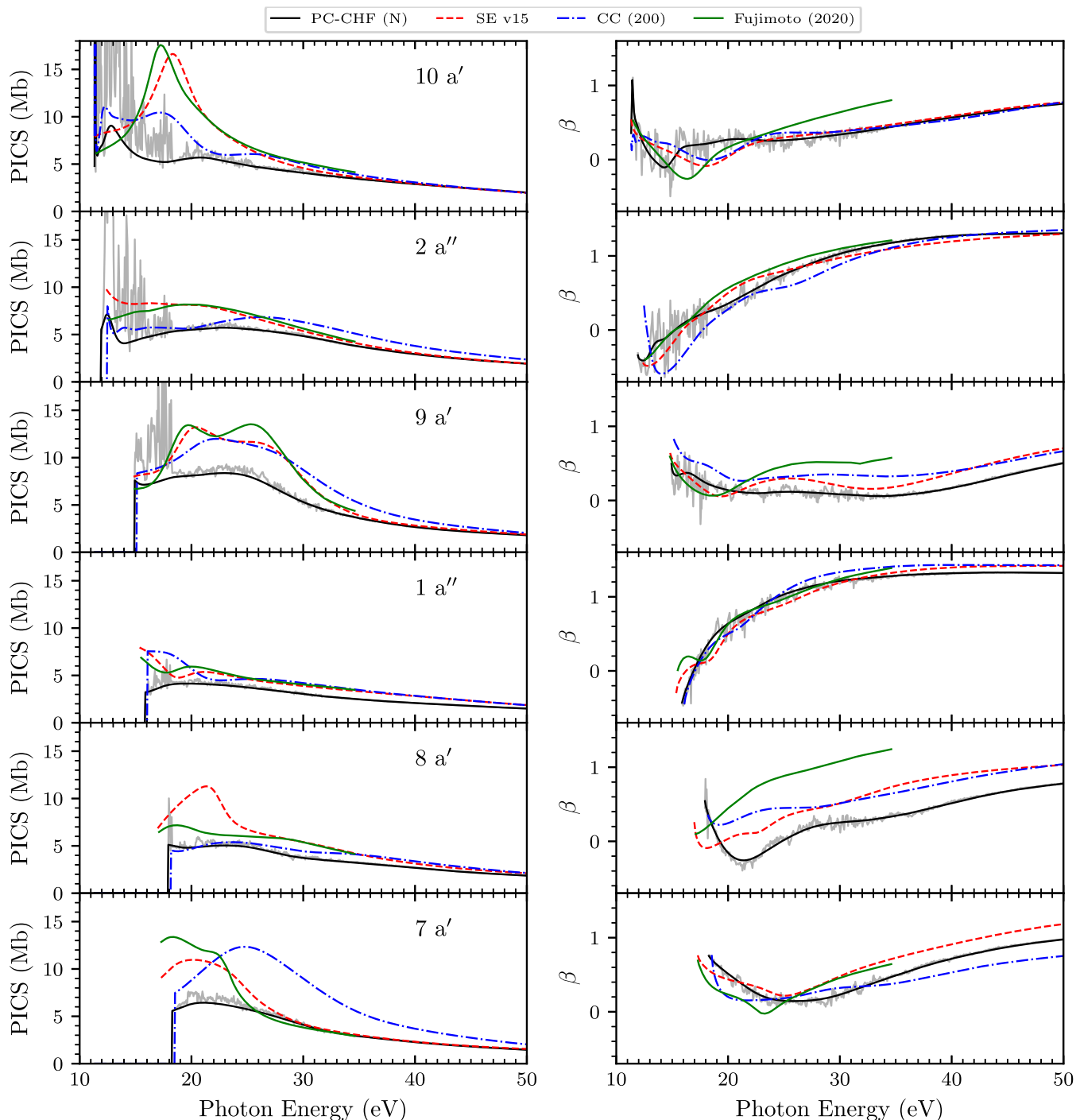


Figure 10. Formic acid photoionization cross-section (left panels) and asymmetry parameters (right panels) for transitions that correspond to ionizing the $10 a'$, $2 a''$, $9 a'$, $1 a''$, $8 a'$ and $7 a'$ orbitals. The smoothed (black solid) and raw (light grey) results of the PC-CHF(N) calculation are compared with the SE results (red dashed), 200-state CC results (blue dot-dash) and the ePolyScat-D calculations (green solid) of Fujimoto *et al* (2020).

4. Conclusion

We have introduced a new R-matrix model, PC-CHF, which rectifies issues associated with the existing SEP model when applied to photoionization of neutral molecules. By coupling the polarization states to their respectively implied ionic states we have eliminated spurious resonances generated by the SEP

model. We have applied the PC-CHF model to three different molecules, H_2O , N_2O and formic acid.

For H_2O we found excellent agreement between the PC-CHF model, the sophisticated CC calculations of Benda *et al* (2020) and experimental data. Similarly, for N_2O , we observe good agreement in the total and state-resolved photoionization cross-sections between the PC-CHF model, the CC calculation

of Benda *et al* (2022) and existing experimental measurements. The most significant differences occurred in the state-resolved asymmetry parameters, specifically for the $A^2\Sigma^+$ and $C^2\Sigma^+$ states and we have attributed this to either inaccuracies in the transition dipole moments or the lack of multiply-excited states in the description of the ionic wavefunctions for the PC-CHF model.

For formic acid we carried out CC and PC-CHF calculations. This is due to a lack of previous R-matrix data and no experimental data for state-resolved cross-sections. For the total photoionization cross-section we find good agreement with the experimental data of Leach–Schwell (2002) and the results of our 200 state CC model, although the PC-CHF model appears to under-estimate the total cross-section significantly. In the state-resolved cross-sections and asymmetry parameters the PC-CHF and CC model display broad agreement. Without experimental data to compare against, it is hard to say which of the three theoretical models, PC-CHF, CC and ePolyScat-D is most accurate. However, based on previous agreement of the CC model for N_2O and H_2O it is likely that the CC model provides the most accurate results.

For the most part, we expect the PC-CHF model to perform well when the ionic states of the molecule can be appropriately modelled by HF wavefunctions i.e., those corresponding to single ionization of an electron from an outer-valence orbital. However, as the photon energy increases and begins to probe the inner valence orbitals, this quasi-particle picture starts to break down (Domcke *et al* 1979). This is because electron correlation effects become increasingly important. At this point, it is not possible to think of photoionization as occurring from a specific molecular orbital and this is where CC models offer a significant advantage. The CC model represents target states as combinations of multiply-excited determinants, which is necessary for modelling more complicated ionic states.

In contrast to CAS-based CC models the PC-CHF model reduces the parameter space of the calculation by fixing the type of orbitals and the number of states to be included in the calculation. Obviously, this comes primarily at the cost of reducing the quality of the target states included but as we have demonstrated this is often a reasonable compromise.

A consideration for future work will be to investigate the application of this model to electron–molecule scattering and photoionization of larger molecules. Moreover, we would like to investigate the effect of calculation balancing between the $(N - 1)$ - and the N -electron wavefunctions. Calculation balancing is already a well-known issue in standard electron-scattering SEP calculations (Dora *et al* 2009, Tennyson 2010). It is possible to over-correlate the scattering wavefunction by including too many virtual orbitals into the calculation. This is because the description of the scattering wavefunction is continually improved whilst the target wavefunction remains unchanged. That being said, given that the results of our PC-CHF model for H_2O and N_2O are in broad agreement with experiment, it is unlikely that our results are significantly over-correlated.

Acknowledgments

TM would like to thank Dr Jakub Benda for sharing data from his R-matrix calculations and for his insightful comments on this work. Support of the Czech Science Foundation as the Project GA CR 20-15548Y and support of the PRIMUS program of Charles University as the Project PRIMUS/20/SCI/003 are gratefully acknowledged. Some computational resources were supplied by the Project ‘e-Infrastruktura CZ’ (e-INFRA LM2018140) provided within the program Projects of Large Research, Development and Innovations Infrastructures. This work was also supported by the Ministry of Education, Youth and Sports of the Czech Republic through the e-INFRA CZ (ID: 90140).

Data availability statement

All data that support the findings of this study are included within the article (and any supplementary files).

ORCID iDs

T Meltzer  <https://orcid.org/0000-0003-1740-9550>
Z Mašín  <https://orcid.org/0000-0001-9382-4655>

References

- Banna M S, McQuaide B H, Malutzki R and Schmidt V 1986 *J. Chem. Phys.* **84** 4739–44
- Benda J and Mašín Z 2021 *Sci. Rep.* **11** 11686
- Benda J, Gorfinkiel J D, Mašín Z, Armstrong G S J, Brown A C, Clarke D D A, van der Hart H W and Wragg J 2020 *Phys. Rev. A* **102** 052826
- Benda J, Mašín Z and Gorfinkiel J D 2022 Analysis of RABITT time delays using the stationary multi-photon molecular R-matrix approach (arXiv:2201.04366 [physics.atom-ph])
- Brambila D S, Harvey A G, Mašín Z, Gorfinkiel J D and Smirnova O 2015 *J. Phys. B: At. Mol. Opt. Phys.* **48** 245101
- Braunstein M and McKoy V 1987 *J. Chem. Phys.* **87** 224–8
- Brigg W J, Harvey A G, Dzarasova A, Mohr S, Brambila D S, Morales F, Smirnova O and Tennyson J 2015 *Japan. J. Appl. Phys.* **54** 06GA02
- Brion C E and Tan K H 1979 *J. Electron Spectrosc. Relat. Phenom.* **15** 241–6
- Brundle C and Turner D 1968 *Proc. R. Soc. A* **307** 27–36
- Brundle C R, Turner D W, Robin M B and Basch H 1969 *Chem. Phys. Lett.* **3** 292–6
- Bruner B D *et al* 2016 *Faraday Discuss.* **194** 369–405
- Burke P G 2011 *R-Matrix Theory of Atomic Collisions (Springer Series on Atomic, Optical, and Plasma Physics) vol 61* (Berlin: Springer)
- Carlson T A, Keller P R, Taylor J W, Whitley T and Grimm F A 1983 *J. Chem. Phys.* **79** 97–106
- Dahlström J M, Guénot D, Klünder K, Gisselbrecht M, Mauritsson J, L’Huillier A, Maquet A and Taïeb R 2013 *Chem. Phys.* **414** 53–64
- Domcke W, Cederbaum L S, Schirmer J, von Niessen W, Brion C E and Tan K H 1979 *Chem. Phys.* **40** 171–83
- Dora A, Tennyson J, Bryjko L and van Mourik T 2009 *J. Chem. Phys.* **130** 164307
- Fujimoto M M, Tanaka H K, Marinho R R T, Medina A, Prudente F V and Homem M G P 2020 *J. Phys. Chem. A* **124** 6478–85

- Gianturco F A, Lucchese R R and Sanna N 1994 *J. Chem. Phys.* **100** 6464–71
- Goddard J D, Yamaguchi Y and Schaefer H F 1992 *J. Chem. Phys.* **96** 1158–66
- Haddad G N and Samson J A R 1986 *J. Chem. Phys.* **84** 6623–6
- Harvey A G, Brambila D S, Morales F and Smirnova O 2014 *J. Phys. B: At. Mol. Opt. Phys.* **47** 215005
- Herzberg G 1966 *Electronic Spectra and Electronic Structure of Polyatomic Molecules* (Princeton, NJ: Van Nostrand-Reinhold)
- Hoy A R and Bunker P R 1979 *J. Mol. Spectrosc.* **74** 1–8
- Huppert M, Jordan I, Baykuseva D, von Conta A and Wörner H J 2016 *Phys. Rev. Lett.* **117** 093001
- Leach S, Schwell M, Dulieu F, Chotin J-L, Jochims H-W and Baumgärtel H 2002 *Phys. Chem. Chem. Phys.* **4** 5025–39
- Marante C, Klinker M, Kjellsson T, Lindroth E, González-Vázquez J, Argenti L and Martín F 2017 *Phys. Rev. A* **96** 022507
- Mašín Z, Harvey A G, Spanner M, Patchkovskii S, Ivanov M and Smirnova O 2018 *J. Phys. B: At. Mol. Opt. Phys.* **51** 134006
- Mašín Z, Benda J, Gorfinkiel J D, Harvey A G and Tennyson J 2020 *Comput. Phys. Commun.* **249** 107092
- Modak P and Antony B 2019 *Astrophys. J.* **887** 262
- Morgan L A, Gillan C J, Tennyson J and Chen X 1997 *J. Phys. B: At. Mol. Opt. Phys.* **30** 4087–96
- Nisoli M, Decleva P, Calegari F, Palacios A and Martín F 2017 *Chem. Rev.* **117** 10760–825
- Potts A W and Price W C 1972 *Proc. R. Soc. A* **326** 181–97
- Ruberti M 2019 *J. Chem. Theory Comput.* **15** 3635–53
- Schirmer J, Cederbaum L S, Domcke W and von Niessen W 1978 *Chem. Phys. Lett.* **57** 582–7
- Schmidt V 1992 *Rep. Prog. Phys.* **55** 1483–659
- Schwell M, Leach S, Hottmann K, Jochims H-W and Baumgärtel H 2001 *Chem. Phys.* **272** 77–90
- Schwell M, Dulieu F, Jochims H-W, Fillion J-H, Lemaire J-L, Baumgärtel H and Leach S 2002 *J. Phys. Chem. A* **106** 10908–18
- Smith D G A *et al* 2020 *J. Chem. Phys.* **152** 184108
- Takeshita K 1995 *Chem. Phys.* **195** 117–27
- Tan K H, Brion C E, van der Leeuw P E and van der Wiel M J 1978 *Chem. Phys.* **29** 299–309
- Tennyson J 2010 *Phys. Rep.* **491** 29–76
- Tenorio B N C, Nascimento M A C and Rocha A B 2019 *J. Chem. Phys.* **150** 154308
- Toffoli D and Decleva P 2012 *J. Chem. Phys.* **137** 134103
- Toffoli D and Decleva P 2016 *J. Chem. Theory Comput.* **12** 4996–5008
- Truesdale C M, Southworth S, Kobrin P H, Lindle D W, Thornton G and Shirley D A 1982 *J. Chem. Phys.* **76** 860–5
- Truesdale C M, Southworth S, Kobrin P H, Lindle D W and Shirley D A 1983 *J. Chem. Phys.* **78** 7117–23
- Uzan A J *et al* 2020 *Nat. Photon.* **14** 188–94
- Wang K, Liu J, Zhang H and Liu Y 2021 *Phys. Rev. A* **103** 063101
- Werner H-J, Knowles P J, Knizia G, Manby F R and Schütz M 2012 *Wiley Interdiscip. Rev.-Comput. Mol. Sci.* **2** 242–53